Earth Syst. Dynam., 16, 2201–2223, 2025
https://doi.org/10.5194/esd-16-2201-2025

Earth System Dynamics
Open Access
EGU

Research article

Joint evolution of irrigation, the water cycle and water resources under a strong climate change scenario from 1950 to 2100 in the IPSL-CM6

Pedro Felipe Arboleda-Obando[1,2], Agnès Ducharne[1,2], Frédérique Cheruy[2,3], and Josefine Ghattas[2]

[1]Laboratoire METIS (UMR 7619, Sorbonne Université, CNRS, EPHE), Paris, France
[2]Institut Pierre Simon Laplace (FR 636, Sorbonne Université, CNRS), Paris, France
[3]Laboratoire de Météorologie Dynamique-IPSL, CNRS/Sorbonne Université/École Normale Supérieure-PSL Université/École Polytechnique-Institut Polytechnique de Paris, Paris 75005, France

Correspondence: Pedro Felipe Arboleda-Obando (pedro-felipe.arboleda-obendo@univ-grenoble-alpes.fr)

Received: 9 December 2024 – Discussion started: 18 February 2025
Revised: 22 October 2025 – Accepted: 6 November 2025 – Published: 10 December 2025

Abstract. Irrigation, a key activity for food security, uses local water resources to increase evapotranspiration, creating feedback loops with the atmosphere and water resources. With climate change, it is unclear how irrigation will evolve in the future and how it may influence the evolution of water resources and the water cycle. It is also unclear whether irrigation may be constrained by climate change or water resource shortages. Here, we compare two surface-atmosphere simulations performed with the IPSL-CM6 model from 1950–2100: one with irrigation and one without irrigation. In both simulations, the evolutions of atmospheric radiative forcing, land use, and irrigated areas are taken from CMIP6, which uses a historical dataset for the data before 2014 and the SSP5-RCP8.5 dataset for data after 2014. The two simulations reveal strong global warming and precipitation increases between 1950–2000 and 2050–2100 average values (+5.6 °C and +8.1 %, on average, over land with irrigation). Over the same period, our results indicate an increase in irrigation (+76 % increase in irrigation in the 2050–2100 compared to the 1950–2000 period), which is in line with an important expansion of irrigated areas. The influence of irrigation on evapotranspiration in irrigated areas is greater in 2050–2100 than in 1950–2000 (+12 % vs. +8 %, respectively). Evapotranspiration has also been found to increase in non-irrigated areas near irrigated zones owing to an increase in precipitation under historical and future climate conditions. Water depletion due to irrigation is more intense in the future than in the historical period, although climate change increases water storages and river discharge due to more precipitation in the future. We also identified areas where future environmental conditions can limit irrigation or where irrigation can increase tensions over water use (approximately one-third of irrigated areas, including the Mediterranean basin, California, and Southeast Asia). Our results highlight the importance of considering irrigation in climate projections and future water resources assessments.

1 Introduction

Irrigation supports approximately 43 % of the world's production on approximately 20 % of arable land (Grafton et al., 2017; Siebert and Döll, 2010). As a direct consequence, 70 % of human water withdrawal is used for irrigation (between 2657 and 3594 $km^3\,yr^{-1}$ in 2000; Pokhrel et al., 2016a). The key role that irrigation plays today in food production and the corresponding water demand is the result of an important increase in the irrigated area during the 20th century (a fivefold increase between 1900 and 2005; Siebert et al., 2015a). This expansion of irrigation may continue in the future, as the replacement of rainfed cropping systems with irrigated systems is one of the measures used to adapt agriculture to climate change (Okada et al., 2018).

In addition to its beneficial effects on food production, irrigation has a direct effect on water and energy balances and surface and subsurface hydrology (Döll et al., 2012; Taylor et al., 2013). Such effects can even drive the evolution of certain variables over time (Al-Yaari et al., 2022; Vicente-Serrano et al., 2019). In addition, the increase in evapotranspiration (ET, due to increased crop transpiration and higher near-surface soil moisture) also induces atmospheric feedback loops such as air temperature cooling (Thiery et al., 2020) and changes in precipitation patterns at different scales that affect the water cycle (Al-Yaari et al., 2019; Cook et al., 2015; Guimberteau et al., 2012b; Lo and Famiglietti, 2013; de Rosnay et al., 2003; de Vrese et al., 2016a).

With the acceleration of climate change, there are concerns related to the future of irrigation, as well as its effects on water resources under a changing climate. This has led to global projections (Wada et al., 2013a; Khan et al., 2023a) via global hydrology models (GHMs). However, these modeling efforts with GHMs prescribe atmospheric forcing, so the interaction between irrigation and the atmosphere is not considered.

To consider joint projections for water resources, irrigation, and climate, irrigation must be represented in land surface models (LSMs) within Earth System Models (ESMs), and the LSM must be run in coupled mode with an atmospheric model (McDermid et al., 2023). In recent years, many LSMs have included irrigation modules, such as ORCHIDEE (Yin et al., 2020; Arboleda-Obando et al., 2024a), CLM (Leng et al., 2013; Yao et al., 2022), ISBA-SURFEX (Druel et al., 2022), and MIROC (Pokhrel et al., 2012, 2015). While some of these LSMs have been used in coupled mode under a historical climate (see Al-Yaari et al., 2022a), coupled simulations under a future climate scenario are less common (Cook et al., 2020). This means that the coupled evolution of irrigation activities, water resources, and climate under a future climate change scenario needs to be further explored.

Here, we present the results of a pair of coupled simulations using the Institut Pierre Simon Laplace Climate Model 6 (IPSL-CM6), the version used for the Coupled Model Intercomparison Project phase 6 (CMIP6). In Sect. 2, we present the atmospheric and land surface components of the IPSL-CM6, including the main characteristics of the irrigation scheme; then, we present the modeling setup and analysis methods. In Sect. 3, we explore how irrigation rates are expected to evolve from 1950–2100. We then evaluate the evolution of the influence of irrigation on variables related to the water cycle and water resources. We also explore the limits to irrigation growth under future hydroclimate conditions to identify areas where tensions over water use might increase due to irrigation or where irrigation expansion could be possible. Finally, we discuss the limitations of our results and their implications for climate projections and water resources assessments under future climate conditions.

2 Methodology

2.1 LMDZOR model

We used the LMDZOR model (Cheruy et al., 2020), which involves the coupling of the atmosphere and land components of the IPSL-CM, respectively the LMDZ (Laboratoire de Météorologie Dynamique with Zoom capacity) and ORCHIDEE (Organising Carbon and Hydrology In Dynamic Ecosystems) models. This version uses the LMDZ6A atmospheric model (Hourdin et al., 2020; Sadourny and Laval, 1984) embedded in IPSL-CM6A-LR (Boucher et al., 2020), but we used a medium resolution rather than the standard low resolution (MR and LR, respectively), i.e., 256×256 grid cells, approximately $1.41° \times 0.71°$ in size, and 79 vertical levels. Except for the resolution, the configuration remains close to the model used for CMIP6.

The LMDZ model uses a finite difference discretization of the primitive meteorology equation on an Arakawa C grid, favoring the conservation of entropy rather than that of energy (Boucher et al., 2020). It can refine the grid in both longitude and latitude, and the Z in LMDZ indicates its zoom capabilities. Apart from the dynamics, the model couples physical parameterizations of different processes through a generic interface that computes the vertical transfer of those physical processes. The LMDZ6A version includes important improvements in several processes: it computes eddy diffusion by introducing prognostic turbulent kinetic energy (TKE), with particular attention given to the representation of very stable boundary layers over ice sheet plateaus and boreal lands. It also includes a boundary layer convection module, represented by a thermal plume model, with a time implicit scheme and upwind space finite volume scheme for numerical stability and a better representation of stratocumulus clouds. Finally, it also includes a new deep convection module that assumes coupling between shallow convection and deep convection at the cumulus base level, with a statistical estimate of the maximum vertical velocity (Hourdin et al., 2020).

The ORCHIDEE land surface model describes the mass, momentum, and heat fluxes between the surface and the atmosphere (Krinner et al., 2005). The version used here corresponds to ORCHIDEE 2.2, which is similar to the ORCHIDEE 2.0 model used in CMIP6 (Boucher et al., 2020; Cheruy et al., 2020) but includes some minor bug corrections and a global irrigation scheme that was recently developed and evaluated (Arboleda-Obando et al., 2024). The soil column was set to a depth of 2 m, but we used a version with 22 layers instead of 11 layers, so the soil humidity in the root zone defined for the irrigation scheme was finely modeled. ORCHIDEE has been extensively described elsewhere, and we summarize here the main characteristics of the model.

The turbulent fluxes between the surface and atmosphere use the Monin–Obukhov theory and the bulk formulations proposed by Louis et al. (1982). However, the stability functions for the calculations of the surface drag coefficients proposed Louis et al. (1982) are replaced by functions proposed by (King et al., 2001) to better represent stable conditions (Vignon et al., 2017). Additionally, the computation of the surface roughness height has been improved by introducing a dynamic roughness height. Vegetation is represented by 15 plant functional types (PFTs, including bare soil), each with different parameter values to simulate photosynthesis and carbon allocation; carbon fluxes and plant phenology are controlled by the STOMATE (Saclay Toulouse Orsay Model for the Analysis of Terrestrial Ecosystems; Krinner et al., 2005) module, which computes the evolution of the leaf area index (LAI). Note that no specific crop phenology module was used, following Arboleda-Obando et al. (2024), owing to a lack of ubiquitous parameters at the global scale. It means that C_3 and C_4 crops are assumed to have the same phenology as natural grasslands but with higher carboxylation rates. Remark that this simplification may have an impact on the timing and volume of total water withdrawal, by inducing an overestimation of water demand and ultimately water use (if there is available water offer; Arboleda-Obando et al., 2024). This is due to the lack of representation of the crop calendar, including the harvest stage, which keeps the leaf area index values high in the model.

Evapotranspiration follows a classical bulk aerodynamic approach with four subfluxes: snow sublimation, interception loss, bare soil evaporation and transpiration. There are three soil tiles according to vegetation type (bare soil, forest, and crops and grasses) within each grid cell. Surface infiltration is represented as a sharp wetting front based on the Green and Ampt model, whereas vertical soil flow is represented by a 1-D Richards equation (D'Orgeval et al., 2008; Tafasca et al., 2020). The soil is assumed to be homogenous inside the grid cell and is represented by the dominant USDA soil texture according to the map from Zobler (1986). While lateral fluxes between grid cells are neglected, a routing scheme transfers surface runoff and drainage from land to the ocean through a cascade of linear reservoirs (Guimberteau et al., 2012a; Ngo-Duc et al., 2007). Each grid cell is split into transfer units (also called subbasins) with the river reservoir and two local reservoirs: overland and groundwater. Subbasins are defined according to a flow direction map from Vörösmarty et al. (2000) and are enhanced over the polar region by Oki et al. (1999). Note that owing to the coarse resolution, it is possible to have more than one transfer unit inside every grid cell.

While the water balance is independent for each soil tile, the energy balance is the same for the whole grid cell. The surface energy and water budget computation time are the same as that of the atmospheric model, which is 15 min. The routing scheme also uses a 15 min time step (the standard is 1 d) to finely follow changes in reservoirs due to water withdrawal. In contrast, the carbon and plant phenology computed by STOMATE uses a daily time step.

2.2 Irrigation scheme

The irrigation scheme used here was tested and evaluated in Arboleda-Obando et al. (2024a) at the global scale. This work included a sensitivity analysis to understand the effect of each parameter on irrigation volume and evaporation increase, leading to choosing a set of globally homogenous parameters enabling a good match between simulated and reported values of global irrigation withdrawal. Here, we briefly describe its main characteristics. First, the root zone depth is set according to a user-defined parameter. In our case, we set this depth to 0.65 m (11 layers). This depth comprises approximately 90 % of the crop root system as represented in ORCHIDEE. Then, at each time step, the scheme calculates a soil moisture deficit. This deficit is the difference between the actual soil moisture and a user-defined target in all the root zone layers. We set this target to 0.9 times the soil moisture at field capacity. Third, we calculate the irrigation requirement using the prescribed fraction of irrigated grid cells and limit the maximum irrigation per hour to $3\,\mathrm{mm\,h^{-1}}$.

In the fourth step, the module estimates the available water in the natural reservoirs (overland, groundwater, and river reservoirs), with two constraints: a factor to prevent total depletion of the natural reservoir and mimic an environmental flow (set to 0.9 for all three reservoirs) and the facility for accessing the natural reservoir as represented by a prescribed map of irrigated areas that are equipped for surface or groundwater use (Siebert et al., 2010). The facility of water access helps to prioritize one reservoir over others; for instance, in a gridcell with irrigation demand and groundwater availability but no groundwater access infrastructure, all the water supply will come from the surface reservoirs (overland and stream). More details can be found in Arboleda-Obando et al. (2024). Apart from the local reservoirs, the scheme allows river water adduction from local transfer units (also called subgrid basins in Ngo-Duc et al., 2007) within the grid cell, limiting the available water with a factor set here to 0.05 to prevent river depletion. Owing to the coarse scale, water adduction from neighboring grid cells is deactivated.

In the final step, the scheme estimates the maximum water requirement and water supply (locally available water and adduction) and withdraws the volume from the natural reservoirs. The withdrawn water is added at the soil surface for infiltration, thus resembling a flood or drip irrigation technique. This implies that not all of the water volume is involved in transpiration or bare soil evaporation, as the model decides if part of this volume becomes surface runoff or groundwater recharge. The scheme does not represent paddy rice as a different irrigation technique and uses global homogenous parameters taken from Arboleda-Obando et al. (2024a).

We note here some shortcomings identified in the irrigation scheme used here (Arboleda-Obando et al., 2024). The scheme represents a single irrigation technique (the flood technique), and uses a set of simplified rules to trigger irrigation and allocate available water. Besides, the scheme uses

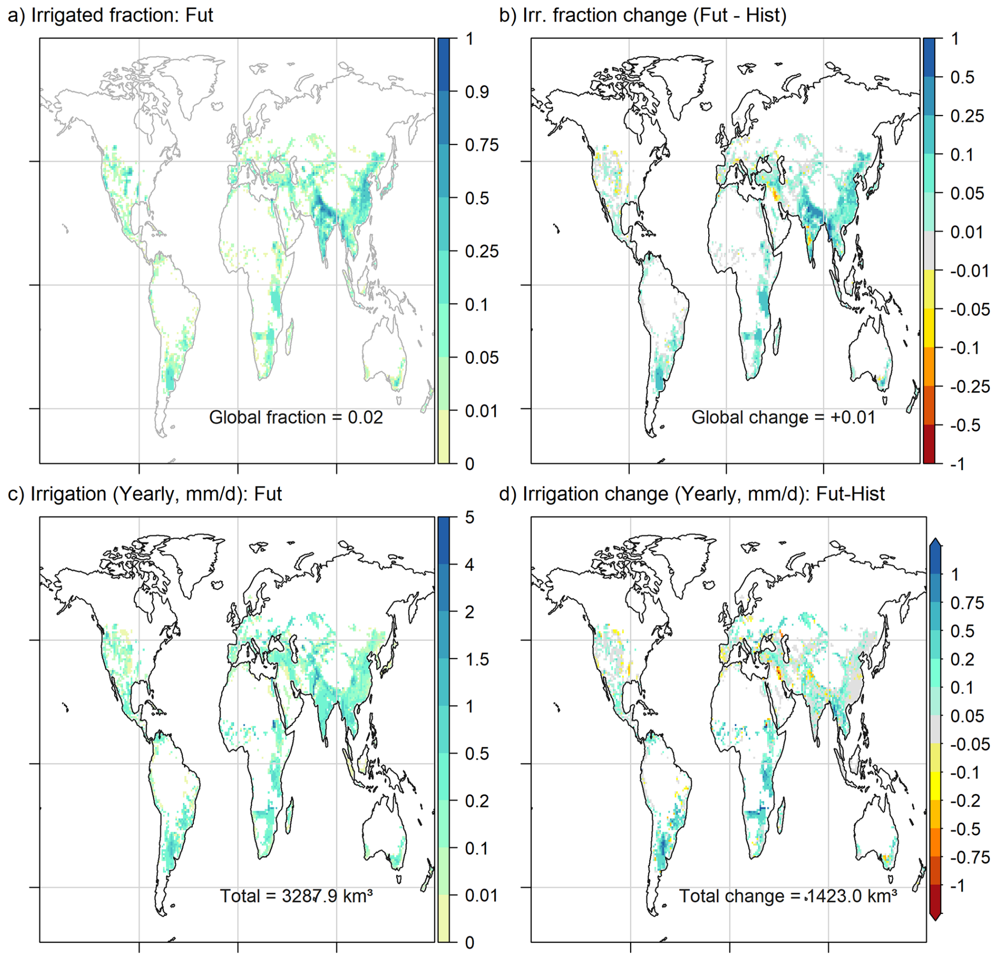

Figure 1. **(a)** Map of the average irrigated fraction by grid cell for the future period (2050–2100). **(b)** Map of the change in the average irrigated fraction by grid cell between the future (2050–2100) and historical (1950–2000) periods. The white areas correspond to grid cells with no irrigated fraction. The irrigated fractions are prescribed by the LUHv2 dataset and interpolated to the model resolution. **(c)** Map of the yearly average irrigation for the future period (2050–2100). **(d)** Map of the change in the yearly average irrigation amount between the future (2050–2100) and historical (1950–2000) periods. The white areas correspond to grid cells with no irrigation.

a joint representation of rainfed and irrigated crops within the same tile, and the scheme doesn't represent conveyance losses. To restrain in part the effect of these shortcomings on estimated irrigation volumes, parameter values were tuned by fitting the simulation to reported irrigation datasets. But we must also note that this parameter tuning is overly simplistic, as it uses globally uniform parameters. Despite these limitations the irrigation scheme produces acceptable estimates of yearly estimation withdrawals at global scale, but tends to underestimate irrigation withdrawals in China, India and the USA, corresponding to the irrigation hotspots (Arboleda-Obando et al., 2024).

2.3 Radiative forcing and socioeconomic scenario

We ran two simulations, one without the irrigation scheme (NoIrr simulation) and a second with the irrigation scheme activated (Irr simulation), for the period 1950 to 2100. Each simulation runs 50 years of spin-up with a prescribed sea surface temperature/sea ice content (SST/SIC) from the AMIP dataset and historical radiative forcing.

The radiative forcing is prescribed using historical (1950–2014) and SSP5-RCP8.5 (2015–2100) datasets from ScenarioMIP (Tebaldi et al., 2021). The use of scenario SSP5-RCP8.5 could be seen as the upper boundary of potential climate change impacts and results in a strong global warming and important changes in precipitation. The use of this scenario allows for analysis of the interaction between irrigation and climate in a context of strong climate change signals and important changes in irrigated land area. For oceanic conditions, the simulations were run with a prescribed bias and variance-corrected SST/SIC dataset (Beaumet et al., 2019) constructed on the basis of the SST/SIC simulated by the fully coupled IPSL-CM6 and observed AMIP. This fully coupled simulation uses historical and SSP5-RCP8.5 data to pre-

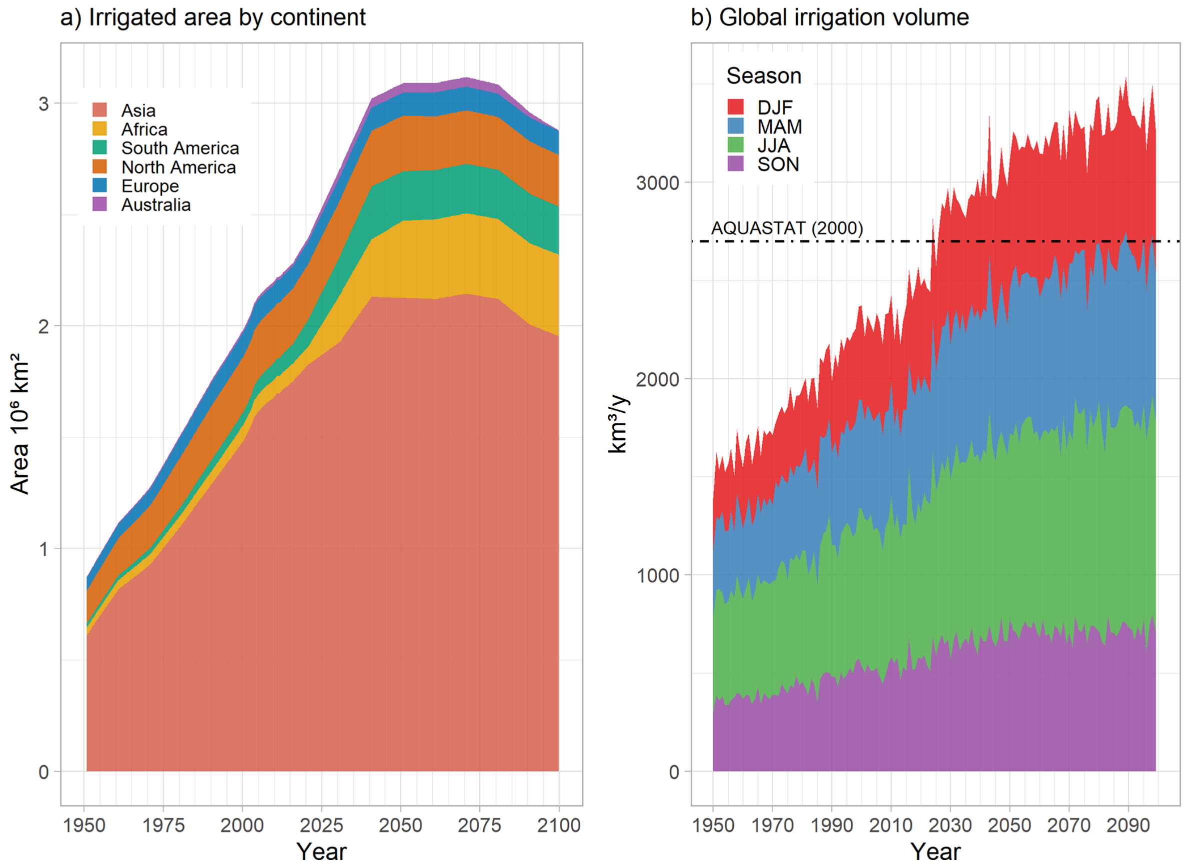

Figure 2. **(a)** Total irrigated area and by continent prescribed by LUHv2. **(b)** Total and seasonal irrigation volume at the global scale simulated by IPSL-CM6 in the Irr simulation. The black line represents the value reported by AQUASTAT around the year 2000 (Frenken and Gillet, 2012).

scribe radiative forcing as well. The unbiased reference is taken from the AMIP dataset.

The land use is prescribed for each year using the Land Use Harmonization 2 (LUHv2) (Hurtt et al., 2020) dataset from the Coupled Model Intercomparison Project 6 (CMIP6); we used the historical and SSP5-8.5 scenarios for 1950–2014 and 2015–2100, respectively. Changes in land use include changes in cropland area (Figs. S1 and S2 in the Supplement). Each year of irrigated area per grid cell is also prescribed with LUHv2, using the same setup (historical and the SSP5-8.5).

The average spatial distribution of irrigated fractions for the 2050—2100 period (Fig. 1a) includes the current hot spots (India, China, Southeast Asia, and the USA) in addition to new hot spots in Africa (Southeast Africa) and South America (Rio de la Plata area). Changes in the irrigated fraction between the future (2100–2050) and the historical (2000–1950) periods show a strong increase in the irrigated fraction in the new hotspots (Africa and South America) and in northern India and Southeast Asia (Fig. 1b), but Asia remains the main hotspot of irrigated areas (Fig. 2a).

Note that some areas do not depict major changes or that the irrigated area even decreases (Iraq and some areas in the Mississippi River Basin). Additionally, scenario SSP5-8.5 assumes that the ratio of irrigated area to cropland area increases (Fig. S2), despite an increase in cropland area, indicating a greater role for irrigation in agriculture and food production. To prescribe the factors of facility of access, we used the Siebert et al. (2010a) map of the fraction of irrigated area equipped with surface water, following Arboleda-Obando et al. (2024a). This map is fixed and representative of conditions around the year 2000. This means that there is no adaptation process related to changes in infrastructure, such as a shift from surface water use to groundwater use.

2.4 Analysis tools

We focused on average changes over land, in irrigated areas and in non-irrigated areas, for irrigation as well as important land and atmospheric variables related to the water cycle. Land refers here to all continental areas except Greenland and Antarctica, which are not represented by the ORCHIDEE LSM. We considered that a grid cell belongs to the